

Article

A Data-Driven Approach to Estimate the Power Loss and Thermal Behaviour of Cylindrical Gearboxes under Transient Operating Conditions

Matteo Autiero *, Marco Cirelli, Giovanni Paoli and Pier Paolo Valentini 

Department of Enterprise Engineering, University of Rome Tor Vergata, 00133 Roma, Italy

* Correspondence: matteo.autiero@uniroma2.it

Abstract: This paper proposes an innovative methodology to estimate the thermal behaviour of the cylindrical gearbox system, considering, as a thermal source, the power loss calculated under transient operating conditions. The power loss of the system in transient conditions is computed through several approaches: a partial elasto-hydrodynamic lubrication model (EHL) is adopted to estimate the friction coefficients of the gears, while analytical and semiempirical models are used to compute other power loss sources. Furthermore, considering a limited set of operating condition points as a training set, a reduced-order model for the evaluation of the power loss based on a neural network is developed. Using this method, it is possible to simulate thermal behaviour with high accuracy through a thermal network approach in all steady-state and transient operating conditions, reducing computational time. The results obtained by means of the proposed method have been compared and validated with the experimental results available in the literature. This methodology has been tested with the FZG rig test gearbox but can be extended to any transmission layout to predict the overall efficiency and component temperatures with a low computational burden.

Keywords: gear transmission system; efficiency of transmission; numerical simulation; neural network; partial EHL



Citation: Autiero, M.; Cirelli, M.; Paoli, G.; Valentini, P.P. A Data-Driven Approach to Estimate the Power Loss and Thermal Behaviour of Cylindrical Gearboxes under Transient Operating Conditions. *Lubricants* **2023**, *11*, 303. <https://doi.org/10.3390/lubricants11070303>

Received: 26 June 2023
Revised: 7 July 2023
Accepted: 18 July 2023
Published: 20 July 2023



Copyright: © 2023 by the authors. Licensee MDPI, Basel, Switzerland. This article is an open access article distributed under the terms and conditions of the Creative Commons Attribution (CC BY) license (<https://creativecommons.org/licenses/by/4.0/>).

1. Introduction

In a general context of fuel consumption reduction and emission minimisation, the evaluation and enhancement of components efficiency have been key in the design and development of mechanical systems. Power loss is strongly affected by the thermal behaviour of the system. Therefore, it is crucial to provide reliable and efficient predictive models to assist engineers in the design phase.

The thermal assessment of closed equipment is generally based on the balance between different sources of energy loss and the heat transmitted to the environment [1]. Gearbox power losses are made up of gear, bearing, seals, and auxiliary losses. Gear and bearing losses can be divided further into no-load losses which occur even without power transmission (bearing drag, gear churning, and windage losses) and load-dependent losses (sliding and rolling for both gears and bearings) which are a function of the power transmitted [2]. A plethora of studies are available in the literature on each power waste mechanism that occurs in gearboxes. The gears, generally the major loss component, must be accurately modelled to provide precise modelling of transmission losses. Deep knowledge of the contact force models is needed to estimate the power loss correctly. In general, the contact force depends on the contact surfaces and the material properties. In the literature, several contact force models can be found [3,4]. To this extent, many researchers provide gear models for the evaluation of contact force and efficiency for ordinary [5] and epicyclic [6,7] gear trains.

Regarding the thermal characterisation of mechanical transmission, the thermal network approach represents one of the most commonly adopted methods. Changenet et al. [8]

proposed the thermal network method coupled with analytical models of power loss predictions to establish the efficiency of a six-speed manual transmission. Their methodology was even applied to the FZG test rig [9], validating experimental results under steady-state and transient operating conditions. More recently, Zhou et al. [10] define a novel thermal network model to predict the tooth contact temperature of the teeth, establishing that contact temperatures decrease with increasing tooth width, pressure angle, and module, but increase with increasing rotation velocity and input torque.

Considering power loss as a thermal source requires the use of simplified models that can be easily incorporated into thermal simulations to avoid unacceptably increasing the computational burden. These shortcomings could be prevented by using machine learning (ML) algorithms in the form of artificial neural networks (ANN). The network is made up of layers, each of them consisting of multiple nodes (or neurons). The connection between nodes represents a linear transformation of information by weights. The main objective of ANN is to find the best weights to optimise the performance of neural networks. To describe and represent complex nonlinear problems, one can consider deep neural networks (DNNs) that contain multiple hidden layers [11]. Recently, ML techniques are employed in geared systems to predict whine noise generation [12], estimate power loss [13], detect root cracks [14], and forecast faults [15]. Moreover, ML has already been used in tribology from wear predictions [16] to tribodynamic simulation of machine elements [17], where the numerical approach of solving partial differential equations [18] is used to provide a training set for a neural network that can be used in fast and precise guessing. Thus, using this methodology, the power loss prediction models can be as complex and accurate as necessary.

In this framework, this study aims to provide a procedure to efficiently simulate gearbox components temperatures using, as a thermal source, the components' power loss estimated by reduced-order models based on DNN. First, the novel methodology is briefly explained in Section 2. Then, in Section 3, the power loss models used are analysed and the whole predictive model is tested against experimental data to prove its reliability. In Section 4, the structure of the predictive neural network is thoroughly examined, highlighting the creation of the data set. Furthermore, the thermal network approach is reported (Section 5) and the results of the thermal model under transient operating conditions are shown (Section 6).

2. Method

The methodology presented can be divided into three main steps:

1. Power loss evaluation for a single operating condition.
2. Deep neural network training.
3. Insert the trained neural network into a thermal network.

The first phase requires the implementation of models to precisely evaluate each power loss component. These models should be sensitive with respect to component temperature, where possible, to capture the temperature effect on power losses. Once the power loss models are implemented, a design of experiment (DOE) is performed to create a data set, as depicted in Figure 1. This data set (divided into training, validation, and test) is employed in the neural network training. More information about this phase is available in Section 4.

In this way, a reduced-order model (ROM) for power loss estimation (ROM-PL) is created. This ROM-PL can be inserted into a thermal network to reduce the calculation time and guarantee results comparable to an approach that uses the complete power loss model.

This new approach is investigated with the test gearbox of the FZG efficiency rig presented in [19], but it is applicable to any transmission geometry. A scheme of the FZG test rig is depicted in Figure 2. It is made up of a test gearbox and a slave gearbox linked together to generate a power loop. Torque is applied externally using a lever and a set of weights, while rotational speeds are controlled by an electric motor that compensates for

losses in the mechanical system. By employing a torque sensor on the motor shaft and measuring the rotational speed, the total power losses can be determined.

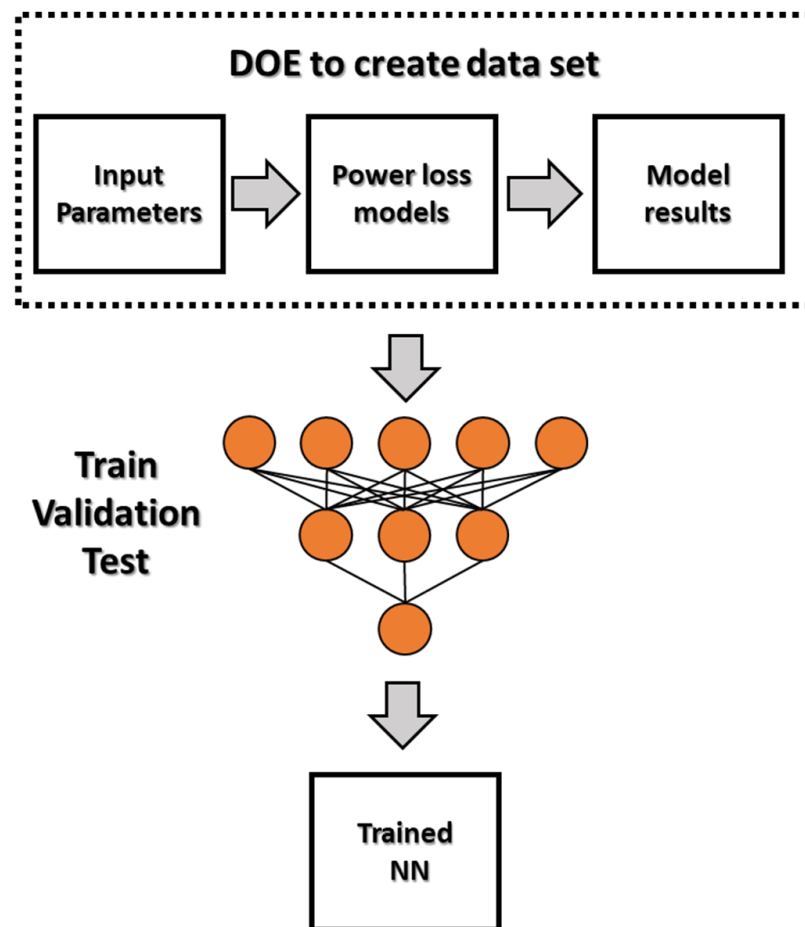


Figure 1. Process to train the power loss predictive neural network.

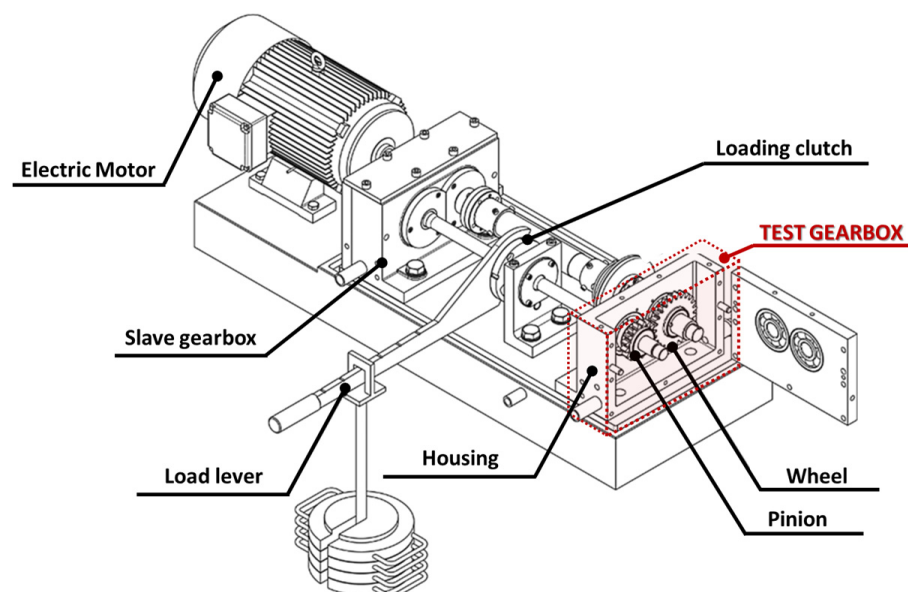


Figure 2. FZG test rig scheme adapted from DIN ISO 14635-1 [20], highlighting in red the gearbox tested in the numerical example.

It is important to clarify that the methodology is intended to be applicable to predict power loss varying only operating conditions (input speed, input torque, and component temperatures), imagining the transmission to be fully defined. Varying the gears, the bearings or the oil type necessarily leads to the creation of a new neural network. Having said that, given the efficient methodology, the process can be repeated for different layouts or varying the oil type, making this procedure useful in the design phase as well.

3. Power Loss Predictions

In gear transmissions, power losses are often divided into load-dependent and no-load contributions. The precise estimation of all power loss addenda is crucial for predicting the heat generated by each component during its operation. According to ISO/TR 1419-2 [21], the total power loss of a geared transmission can be evaluated as

$$P_{TOT} = P_{VZ0} + P_{VZP} + P_{VL0} + P_{VLP} + P_{VD} + P_{VX}, \quad (1)$$

where P_{VZ0} is the churning/windage/squeezing losses of gears, P_{VZP} is the loss associated with tooth friction, P_{VL0} the load-independent loss associated to roller bearings, P_{VLP} is the load-dependent loss of roller bearings, P_{VD} is the power loss due to seals, and P_{VX} represents all the other losses. The power losses considered in this study are described in the following, highlighting the model implied for each term.

3.1. P_{VZP} -Gears Load-Dependent Losses

The losses in meshing involve two components: sliding friction and hydrodynamic rolling. Sliding friction is due to relative motion between gear surfaces, while hydrodynamic rolling loss refers to the power needed to move and compress the lubricant, forming a pressurised oil film that separates the gear teeth. The second is a significant part of the overall system loss, particularly under light loads [22], while at medium to high contact pressures, the first dominates.

Instantaneous power loss due to sliding (P_{VZP_s}) at a generic point along the line of action (x) can be written as

$$P_{VZP_s}(x) = \mu(x)F_n(x)v_{sl}(x), \quad (2)$$

where μ is the friction coefficient, F_n the normal contact force, and v_{sl} the sliding speed all evaluated instantaneously along the contact line. Therefore, to accurately evaluate load-dependent power loss, a loaded tooth contact analysis (LTCA) must be performed to assess the instantaneous contact condition in terms of speed and pressure (i.e., normal force) along the line of action. There are different approaches to calculate the mesh stiffness and, consequently, the contact force along the line of action [23,24]. The semi-analytical model presented in [24] is used to calculate the variation of stiffness along the mesh line and the load shared between the gear teeth. All gear kinematics can be found in the classic gear literature [25]. For the friction coefficient between gears, researchers proposed a plethora of semiempirical models [26]. Among all others, the models by Benedict and Kelley [27] and Höhn [28] are among the most utilised, but in this work, the partial EHL approach presented by Arana et al. [29] is used. The least mentioned focusses on two key aspects: the fluid friction coefficient and the iterative thermal power loss prediction methodology. The friction coefficient is determined using a non-Newtonian rheological model and covers a wide range of viscosity grades. The model is extended to account for partial EHL using the Tallian [30] asperity load share functions. According to Tallian, partial EHL exists when $0.5 < \lambda < 4$, where λ is the specific film thickness ratio, defined by the ratio between central film thickness h_c , and the composite root mean square roughness of the surfaces. Loaded gears (i.e., non-idle) are often assumed to operate under this lubrication regime [29]. This occurrence is the thermal power loss prediction methodology calculates the contact and film temperatures to estimate the traction and film thickness precisely. The models are validated with experimental results, demonstrating accuracy within 10% error. Their

work emphasises the importance of accurately characterising the high-pressure viscosity behaviour of the lubricant for predicting friction coefficients and power losses in gears.

In particular, the friction coefficient μ for partial EHL regimes is defined as

$$\mu = \varepsilon\mu_s + (1 - \varepsilon)\mu_f. \quad (3)$$

Here, μ_f and μ_s represent the coefficients of fluid and solid friction, respectively. The parameter ε represents the ratio of the real contact area to the apparent (Hertzian) contact area and is strictly dependent on λ . For this study, the Doleschel model [31] was used to correlate λ and ε , which is found to be more consistent with experimental data. The common assumption is that the boundary friction coefficient μ_s is unaffected by varying operating conditions [29]. In this application, a value of $\mu_s = 0.0863$ was assumed, in accordance with the experimental observation reported in [19].

Conversely, the fluid friction coefficient μ_f can be written, with all the assumptions made in [29], as

$$\mu_f = \min \left[\frac{2 \cdot \Lambda}{\alpha \cdot \bar{p}} \cdot \sinh^{-1} \left(\frac{\eta \cdot \alpha \cdot V_s}{2 \cdot \Lambda \cdot \Phi_T \cdot h_c} \right), \Lambda \right], \quad (4)$$

where Λ is the limiting-stress pressure coefficient (i.e., twice the product of limiting shear stress and pressure viscosity coefficient), α is the local piezo-viscosity coefficient (evaluated at Hertz contact pressure according to Bair and Winer, [32]), \bar{p} is the mean contact pressure, η is the dynamic viscosity evaluated at the mean contact temperature and pressure (using the so-called “Modulus equation”), V_s is the sliding velocity, and Φ_T is a factor that accounts for the thermal effect on film thickness. All the aforementioned parameters strongly depend on the type of oil and operating conditions. For the equations and the flowchart required for the calculation, the reader can refer to [29].

Regarding rolling traction, the model proposed by Anderson [22] is used. According to his studies, the power loss due to rolling is computed as:

$$P_{VZP_r}(x) = C[\Phi_T(x)h_c(x)v_r(x)FW], \quad (5)$$

where C is a constant of proportionality, v_r is the rolling velocity (i.e., sum of profiles velocity), and FW is the gear face width.

Once the instantaneous loss along the line of action has been calculated, it is possible to evaluate the average power loss as the integral average along the path of contact.

3.2. P_{VZ0} -Gears No-Load Losses (Spin Losses)

Gear no-load power losses can be divided into churning losses, windage losses, and squeeze (or pocketing) losses. Both windage and churning occur in geared transmissions and are complementary to each other. Churning refers to the generation of losses in all oil-bath lubricated gearboxes. At the same time, windage involves the significant involvement of air along with the lubricant, particularly in cases such as large gears lubricated with a thin layer of grease or high-speed gears with injected lubrication. Additionally, squeezing or pocketing is a lesser magnitude phenomenon compared to windage and churning. It occurs when there is a sudden reduction in the volume between the mating surfaces, which causes the lubricant or lubricant mixture to be squeezed out [33]. Niemann [34] provides an estimate of power waste due to churning in dip lubrication conditions i , which can be written for each gear as

$$P_{Z0} = \omega \left(\frac{ev_t^{1.5}FW}{2.72 \cdot 10^{-6}} \right), \quad (6)$$

where ω is the rotational speed, e is the immersion depth, v_t the tangential speed, and FW is the gear face width.

3.3. P_{VL} -Bearing Losses

Bearing friction torque and spin losses are calculated according to the SKF model [35]. It enumerates several types of friction that require consideration including rolling friction (M_{rr}), sliding friction (M_{sl}), friction from seals (M_{seal}), and friction from drag losses (M_{drag}). The calculation for the total friction torque is made by adding all these contributions as

$$M_{tot} = M_{rr} + M_{sl} + M_{seal} + M_{drag}. \quad (7)$$

All torque loss addenda are heavily dependent on bearing type, lubrication condition, and size and for each component one can refer to [35] for all the calculation procedures. To ensure that the model considers the variations in bearing temperature, the oil properties are evaluated at the average temperature between the bearing housing inlet (ϑ_{in}) and outlet temperatures (ϑ_{out}). It is possible to consider the inlet bearing temperature equal to the oil temperature, while for the output temperature, following the SKF instructions available at [36], one can write:

$$\vartheta_{out} = \vartheta_{in} + \frac{P_L - W_s(\vartheta_B - \vartheta_{amb})}{27 \cdot Q}, \quad (8)$$

where P_L represents the power loss in [W], W_s is the total heat dissipation per degree above ambient temperature in [$W/^\circ C$], ϑ_B the bearing temperature in [$^\circ C$], ϑ_{amb} the ambient temperature in [$^\circ C$], Q the oil flow into the bearing. For the oil flow into the bearing, it is possible to use the maximum value, calculated as:

$$Q_{max} = \frac{DB}{12500}. \quad (9)$$

Indicating with D the bearing outer diameter in mm and with B the bearing width in mm.

3.4. P_{VD} : Seal Losses

Radial shaft seals (RSS) are commonly used to seal the shaft end in geared transmission. Their sliding and the consequent power loss depend on various factors, such as the hardness of the shaft surface roughness, the type of sealing, the lubricant type, and temperature [37]. Various manufacturers provide diagrams to determine the friction torque related to RSS. A generally valid relation can be found in [38] where the power loss due to seals (P_{VD}) in W is computed as:

$$P_{VD} = \left[145 - \vartheta_{oil} + 350 \log \left(\log \left(VG_{grade} + 0.8 \right) \right) \right] d^2 n * 10^{-7}, \quad (10)$$

where ϑ_{oil} is the oil operating temperature in $^\circ C$, VG_{grade} is the oil viscosity grade (i.e., nominal kinematic viscosity at $40^\circ C$ in mm^2/s), and n is the rotational speed in rpm.

3.5. Model Validation

Power loss prediction models are tested with experimental data available from [19], where the FZG test rig is tested with different rotational speeds and torque and with three different gear pairs.

For sake of conciseness only the spur gear pair presented in [19] is taken as reference, and the pair geometry and all the gearbox parameters are reported in Table 1, while the models employed for the correlation are summarised in Table 2.

Table 1. FZG rig characteristics reported in [19].

Gears			
Name	Pinion		Wheel
Center distance (mm)		91.5	
Number of teeth	16		24
Normal module (mm)		4.5	
Normal pressure angle (°)		20	
Helix angle (°)		0	
Face width (mm)		14	
Addendum modification coefficient	0.182		0.172
Flank surface roughness (µm)	0.174		0.157
Material		16MnCr5	
Bearings			
Bearing type		Cylindrical roller NU406	
Seals			
Input shaft diameter (mm)		24	
Output shaft diameter (mm)		54	
Oil			
Oil type		Mineral	
Kin. Viscosity@40 °C (mm ² /s)		32.63	
Kin. Viscosity@100 °C (mm ² /s)		5.45	
Density@15 °C (kg/m ³)		876.8	

Table 2. Calculation model for each source of power loss.

Power Loss	Model
Gear sliding	Partial EHL [29]
Gear rolling	Anderson [22]
Gear Churning	Niemann [34]
Bearings	SKF [35]
Seals	Simmering model [38]

As it can be seen in Figure 3, the proposed model shows a good correlation with the experimental data especially at high torque values. On the other hand, at low to medium torque, the model underestimates the loss at high values of rotational speed. This occurrence can be explained by the higher uncertainty of the no-load-dependent losses of both roller bearings and gears. In fact, experimentally derived models such as the one provided by Niemann could be used only as a rough estimate, while a CFD analysis would be required for the most accurate calculation [33]. As a proof, the error remains approximately constant as the torque increases.

Moreover, a different trend distinguishes the total losses at high torque from those at lower torque ones. This is imputable to the dominant loss mechanism depending on the operating condition. Figure 4 shows the total loss divided into each component to better explain this phenomenon. The no-load losses (i.e., P_{Z0} , P_{B0} , and P_{VD}) remain constant varying the output torque, while at high contact pressure gear sliding and load-dependent bearing losses predominate.

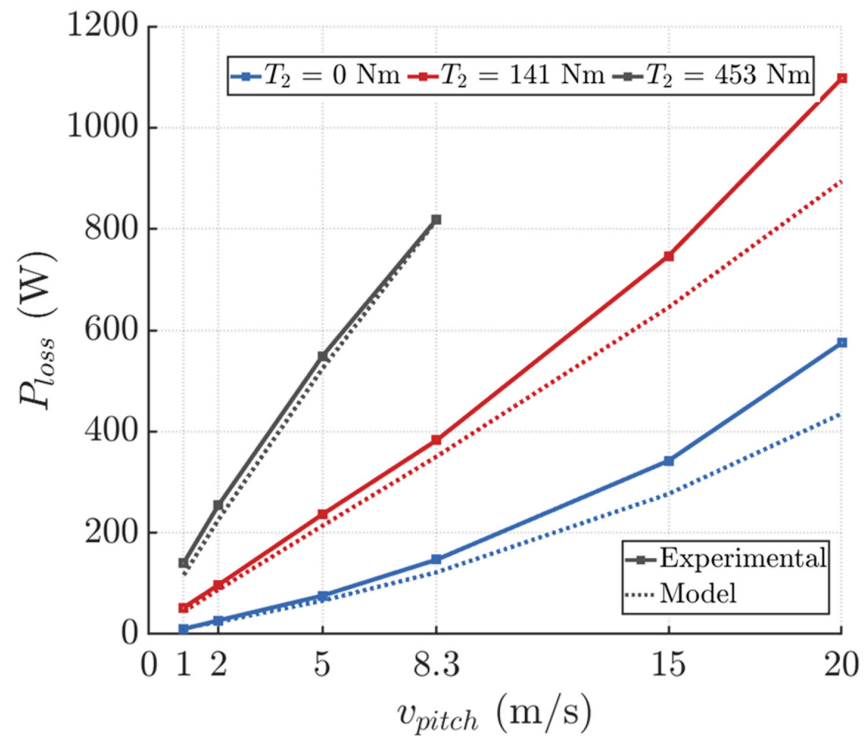


Figure 3. Comparison between the experimental data available in [19] and the proposed model of total power loss against pitch velocity at different output torques.

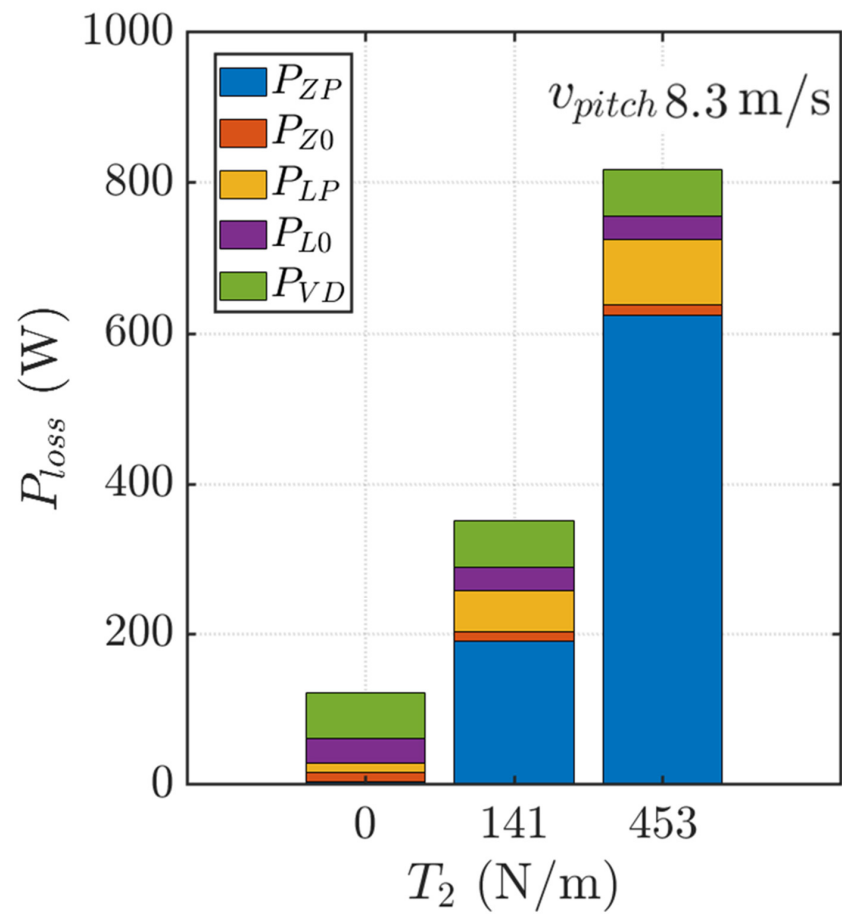


Figure 4. Loss breakdown for a fixed pitch velocity of 8.3 m/s at different output torques.

4. Neural Network Predictors

Once the power loss model is validated, it is possible to train a deep neural network (DNN) to rapidly estimate the power loss for a given operating condition and component temperature. Specifically, feedforward networks (FFNs) with hidden layers and non-linear activation functions are considered. The configuration of DNNs can be further defined by hyperparameters, which include factors like number of layers, number of nodes per layer, batch size, activation functions, and training algorithm. The effectiveness of the DNN is heavily dependent on making the appropriate choice for these hyperparameters.

For this application, the supervised learning approach is employed to build a reduced order model for power loss prediction (ROM-PL).

For this gearbox layout, once the geometry and the oil type are known, it is possible to identify 9 input parameters that have an impact on power waste during transient operation: oil temperature (ϑ_{oil}), pinion, and gear bulk temperature (ϑ_{Bulk1} and ϑ_{Bulk2}), four bearings temperature (ϑ_{Li}), transmitted torque (T), and rotational speed (n). As it could be observed, not all parameters directly influence every power loss component. Therefore, as shown in Figure 5, three small FFNs are used in the power loss prediction: NN_{ZP} for gear sliding and rolling loss, NN_0 for churning and seal losses, NN_B for bearings losses (one per bearing). The choice of hyperparameters is reported in Table 3 and are the same for each neural network.

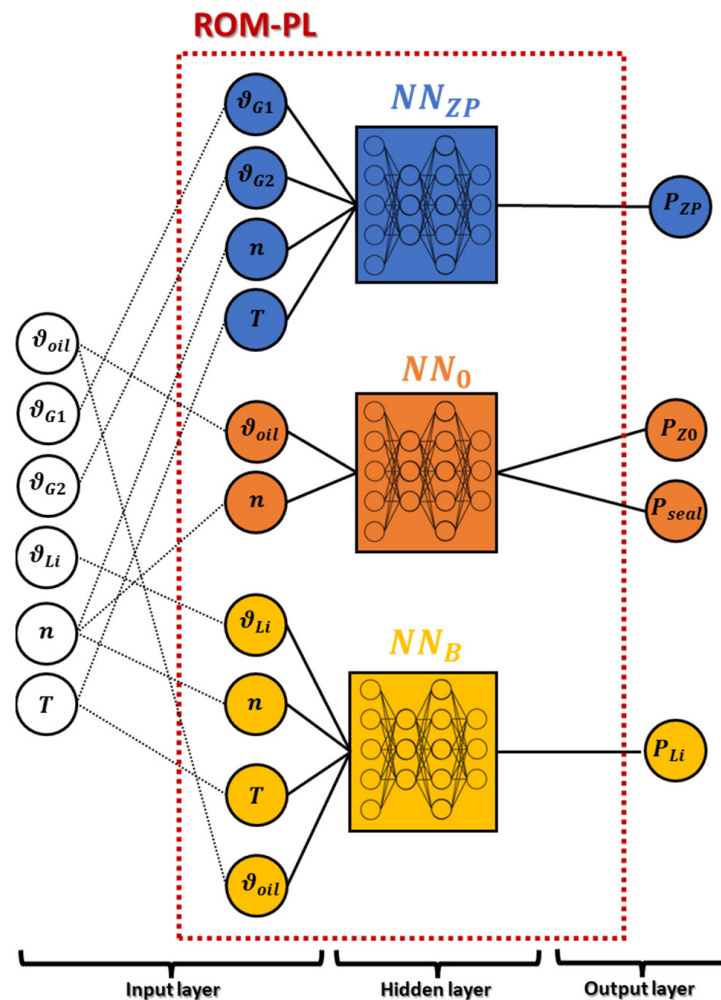


Figure 5. Reduced order model for power loss estimation (ROM-PL).

Table 3. DNN hyperparameters.

Hyperparameters	
Num. of hidden layers	2
Num. of nodes per layer	5
Batch size	64
Num. of epochs	1000
Activation function	Sigmoid
Training algorithm	Levenberg–Marquardt backpropagation

A data set is created for each net evaluating the power loss associated with the varying input parameters performing a design of experiment (DOE). The easiest way to choose a DOE parameters combination is to create a uniform mesh for input parameters, that is, perform a full factorial combination of them. In this way, the number of simulations becomes unsustainable if the parameters are too many or if a good definition is required for each parameter. For this reason, a Latin Hypercube Sampling (LHS) algorithm is utilised for the creation of the data set. LHS is a statistical method for generating a nearly random sample of parameter values from a multidimensional distribution [39].

The main advantage of Latin hypercube sampling (LHS) is that it produces samples that reflect the true underlying distribution and tends to require much smaller sample sizes than simple random sampling [40]. In Table 4, the upper and lower bounds of each input parameter are reported.

Table 4. DOE input parameters bounds.

Parameter	Bounds	Parameter	Bounds	Parameter	Bounds
n (rpm)	[50, 6500]	T_{G1} (°C)	[20, 120]	T_{B2} (°C)	[20, 120]
T (Nm)	[1, 350]	T_{G2} (°C)	[20, 120]	T_{B3} (°C)	[20, 120]
T_{oil} (°C)	[20, 120]	T_{B1} (°C)	[20, 120]	T_{B4} (°C)	[20, 120]

To generate a data set for each NN, a DOE consisting of 400 elements is created. This data set is randomly divided into three groups: a training set, a validation set, and a test set. The training set contains 80% of the data, while the validation set, and the test set contain 10% each.

Additionally, for the predictive performance evaluation of the NNs, another sample of 400 elements is randomly generated within the parameter bounds, and the value of the power loss prediction model is compared with the NN guesses. This set must be different from the data set employed to train the NNs in order to better judge the performance. The evaluation is based on the R-squared value [41] denoted by R^2 . After obtaining an output y for a given test set and a ROM prediction \hat{y} for the same test set, the performance metric is determined as follows:

$$R^2(y, \hat{y}) = 1 - \frac{\sum_1^n (y_i - \hat{y}_i)^2}{\sum_1^n (y_i - \bar{y})^2} \quad (11)$$

where $y = (y_1, \dots, y_N)$, $\hat{y} = (\hat{y}_1, \dots, \hat{y}_N)$, $\bar{y} = \sum_1^n y_i / N$, and N denote the number of data samples of the output y . Here, for simplicity, we assume y is 1-dimensional. As the solution \hat{y} of the ROM predicts the label y more accurately, the value R^2 approaches 1.

As it is possible to observe from Figures 6–8 the neural networks provide extremely good results. In fact, by reporting the normalised (using the min–max normalisation) power loss predicted (\hat{y}) versus the one calculated (y), it is possible to observe an excellent correlation for all the NNs.

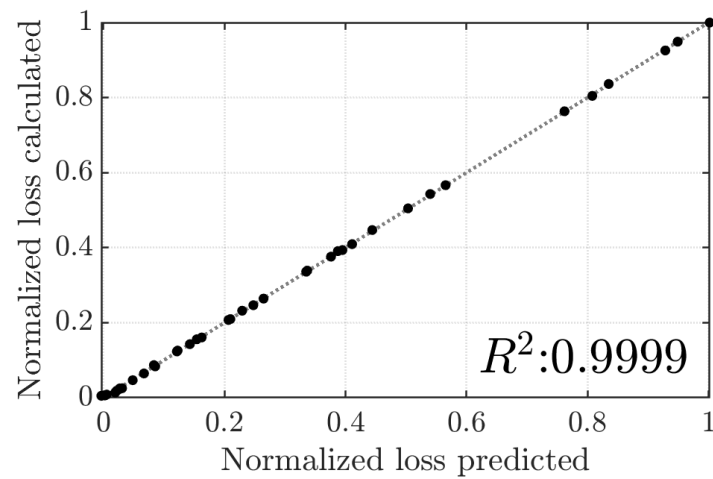
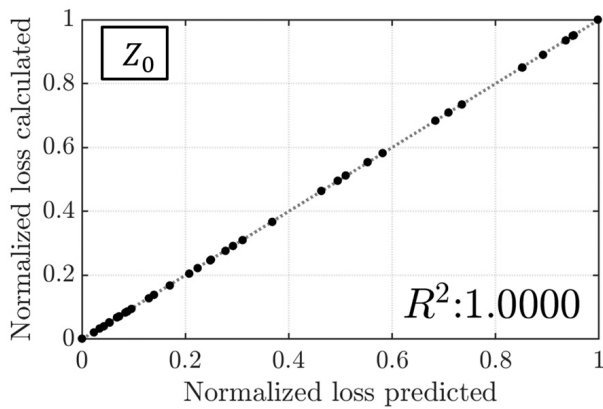
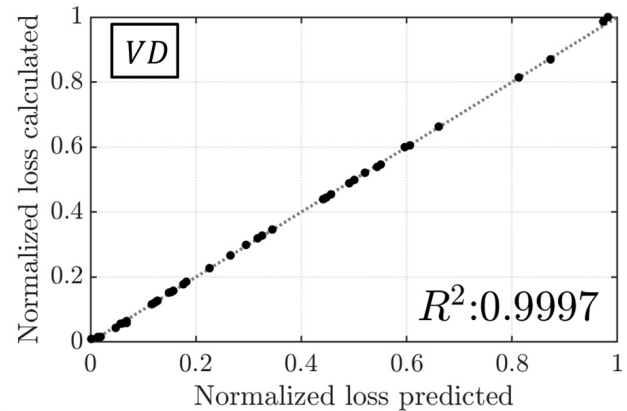


Figure 6. Calculated normalised power loss (sliding and rolling losses) versus normalised power loss predicted (NN_{ZP}).



(a)



(b)

Figure 7. Normalised power loss calculated ((a) churning and (b) seal losses) versus normalised power loss predicted (NN_{Z0}).

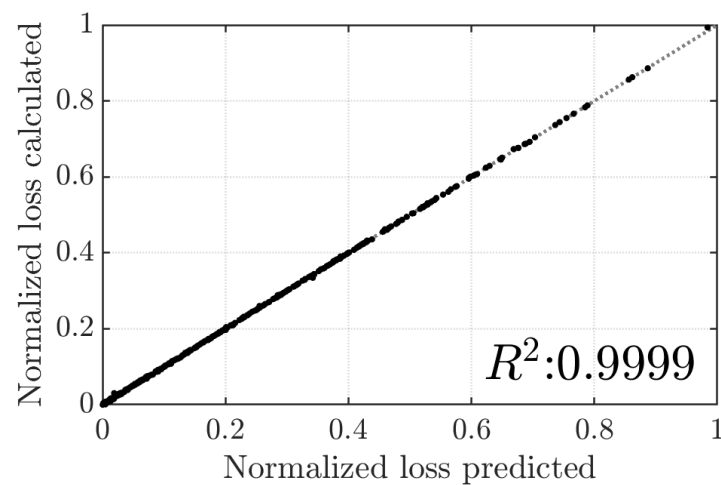


Figure 8. Normalised power loss calculated (bearing losses) versus Normalised power loss predicted (NN_B).

5. Thermal Network

The heat generated in cylindrical gearboxes, due to all power loss sources, is exchanged with the environment by conduction, radiation, and convection. The evaluation gearbox temperatures are of great interest by the means of components durability. In a quasi-stationary state of equilibrium, which means that all operating conditions remain approximately constant, the heat dissipated equals the power loss generated:

$$P_{TOT} = Q,$$

where the heat dissipated is the sum of all heat transmission phenomena.

During a transient operating condition, the presence of a non-null temperature gradient (dT/dt) means that the balance equation must be adapted as:

$$P_{TOT} = Q + mc \frac{dT}{dt},$$

where m is the component mass and c is the component-specific heat capacity.

In this study, the thermal network technique presented in [9] is followed. It consists of identifying isothermal components in the gearbox and appropriately connecting them via thermal resistances evaluated depending on the heat transfer mechanism. The FZG gearbox is divided into 14 isothermal elements and connected with thermal resistances as shown in Figure 9. Each resistance connects different components (represented by lines) and modulates the heat flux through the network.

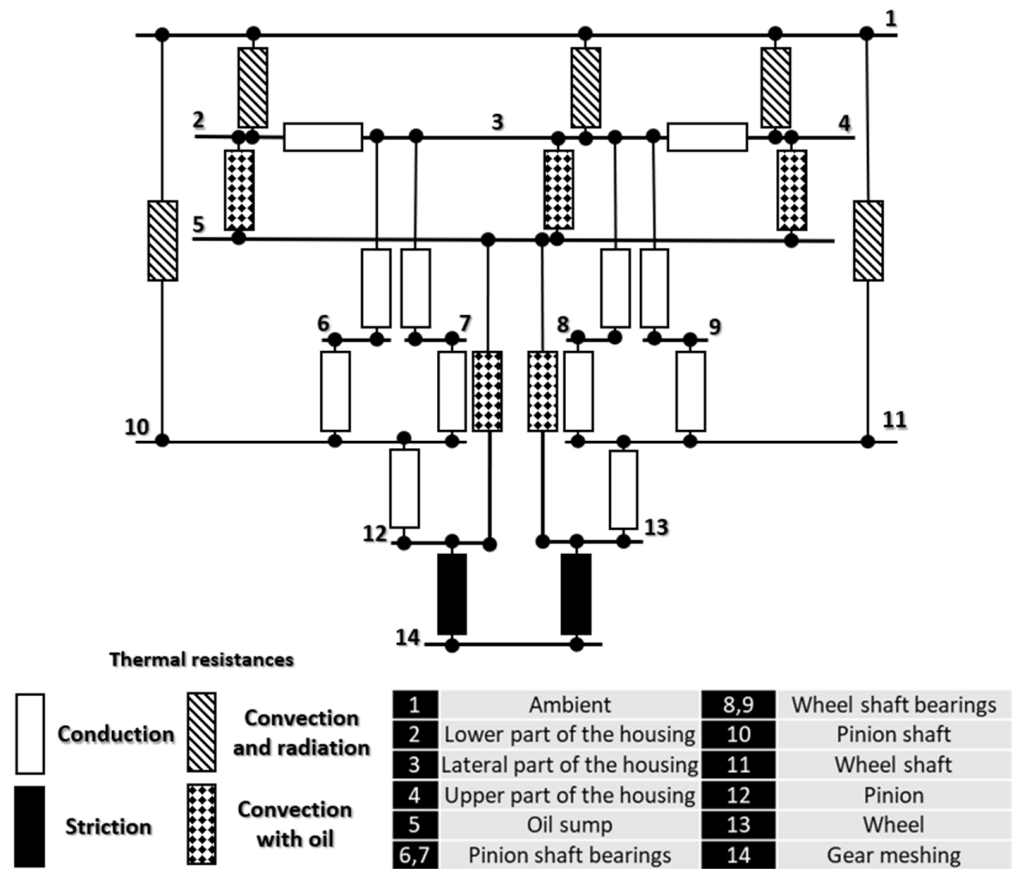


Figure 9. Thermal network of an FZG test rig gearbox. Adapted from [9].

The thermal resistances could be of four different categories: conduction through a metal medium, convection with oil, convection and radiation with air, and striction. The least mentioned occurs in the teeth meshing region due to the size difference between

the Hertzian contact zones (exchange surfaces) and the overall dimensions of the gears. This restriction leads to heat build-up and potential temperature variations within the gear system [42]. Each power loss represents a concentrated heat source acting directly on the system. In particular, referring to the schematisation of Figure 9, the meshing losses represent a heat source for level 14, the bearings losses for levels 6-7-8-9 (depending on the considered bearing), and the no-load losses for level 5 which represent the oil sump.

For a precise calculation step of each thermal resistance, one can refer to [8,9], while the values of the heat transfer coefficient and all geometrical information needed for the development of the thermal network are taken from [19] and reported in Table 5.

Table 5. Parameters for the calculation of thermal resistances.

Parameter	Value
Gearbox outside surface (m ²)	0.214
Gearbox inside surface (m ²)	0.149
Gearbox height (m)	0.215
Wall thickness (m)	0.024
Heat transfer coefficient between oil and housing (W/(m ² ·K))	950
Thermal conductivity of the housing (W/(m·K))	40
Velocity of cooling air (m/s)	2
Temperature of cooling air (°C)	25 ÷ 29
Contact surface of forced cooling air (m ²)	0.214
Length of pinion shaft (m)	0.223
Diameter of pinion shaft (m)	0.024
Length of wheel shaft (m)	0.090
Diameter of wheel shaft (m)	0.055
Thermal conductivity of shafts (W/(m·K))	46

Heat transfer coefficient and thermal conductivity are considered constant with varying operating conditions, even though they are affected by temperature and cooling air velocity. The thermal network model of the FZG test rig is replicated in Matlab[®]/Simulink[®] environment using the built-in Simscape[™] thermal module to simulate the gearbox transient behaviour.

6. Results

The thermal network of the FZG test rig is tested under transient operating conditions. To highlight the improvement in computation time of the approach presented, each heat flux generated by power loss is evaluated with both the full power loss model (F-PL) and the reduced order model (ROM-PL). To simulate the real accuracy of the reduced model under thermal transient conditions, a numerical test with variable input torque values and speeds has been applied. It consists of a 600 s drive cycle characterised by speed and torque profiles depicted in Figure 10. The initial temperature of all components is set to 20 °C to simulate a cold start.

The characteristics of the gearbox under test are the same as the gearbox used for model validation (see Table 1). In the table, details about the gears, the bearing type, the seals, and the lubricant adopted are reported. Moreover, for the churning losses, the gears were dip-lubricated with an oil level of 19 mm relative to the shaft axis.

The power loss during the drive cycle for both the F-PL and the ROM-PL is shown in Figure 11. The comparison shows good agreement between the two approaches, especially after the initial stage. In fact, in this phase, neural networks are predicting the power loss value around the lower limit of all parameters (i.e., the temperatures of the components are close to the lower extreme, as well as the torque and the rotation speed). As proof of this, in the final part, where the operating conditions in terms of torque and speed are similar to the initial ones, the predictions are more appropriate because of the higher component temperatures.

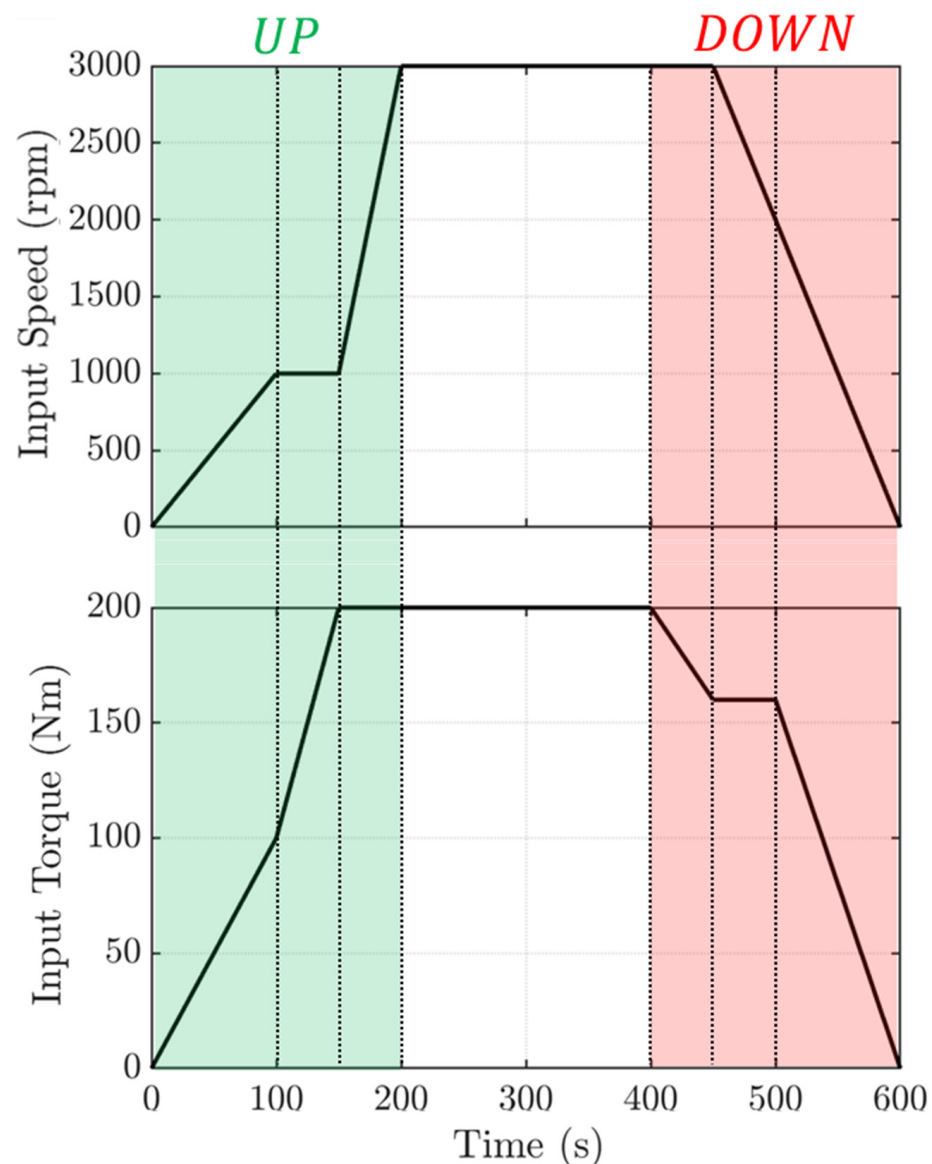


Figure 10. Rotational speed (**up**) and torque (**down**) profiles to simulate transient operating conditions.

Moreover, the effect of temperature variations can be appreciated in the constant power phase. The sliding losses slightly increase with the increasing temperature as a decrease in the result of kinematic viscosity, a consequent lubricant film thinning, and an increase of friction coefficient. This trend is not extremely visible, while the effect on roller bearing losses is contrary and much more noticeable. The lubricant thinning hardly reduces the bearing rolling friction torque (M_{rr}) and, in addition, drag losses decrease because of an increasing oil temperature. This effect is the same visible for no-load losses.

The temperature profile of some main components of the thermal network is reported in Figure 12, where it is possible to see how neural networks operate effectively in temperature estimation. Due to the input power profile utilised, all components experience a heating and cooling phase. From the results, it is evident that the temperature of the gear body is higher when the torque is significant, as the sliding losses represent the primary source of heat. When torque levels drop throughout the cooling phase, the gear body tends to assume the temperature of the oil. Furthermore, the input branch (Shaft 1, B1-B2, and Pinion) exhibits higher temperatures compared to the output branch (Shaft 2, B3-B4, and Wheel) due to the higher rotational speed, which results in greater bearing losses. Finally,

it is observed that the temperature of the shafts is greater than the corresponding bearings because the former are also directly heated by the gears.

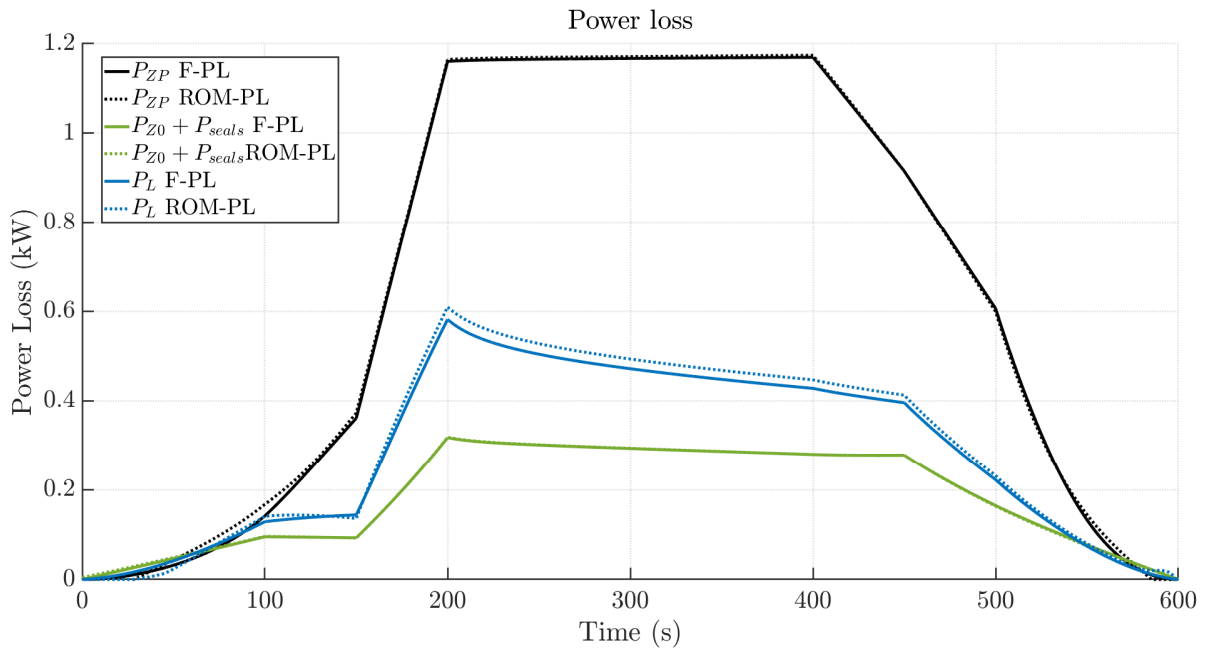


Figure 11. Power loss during the drive cycle. Full power loss model compared with the reduced order model.

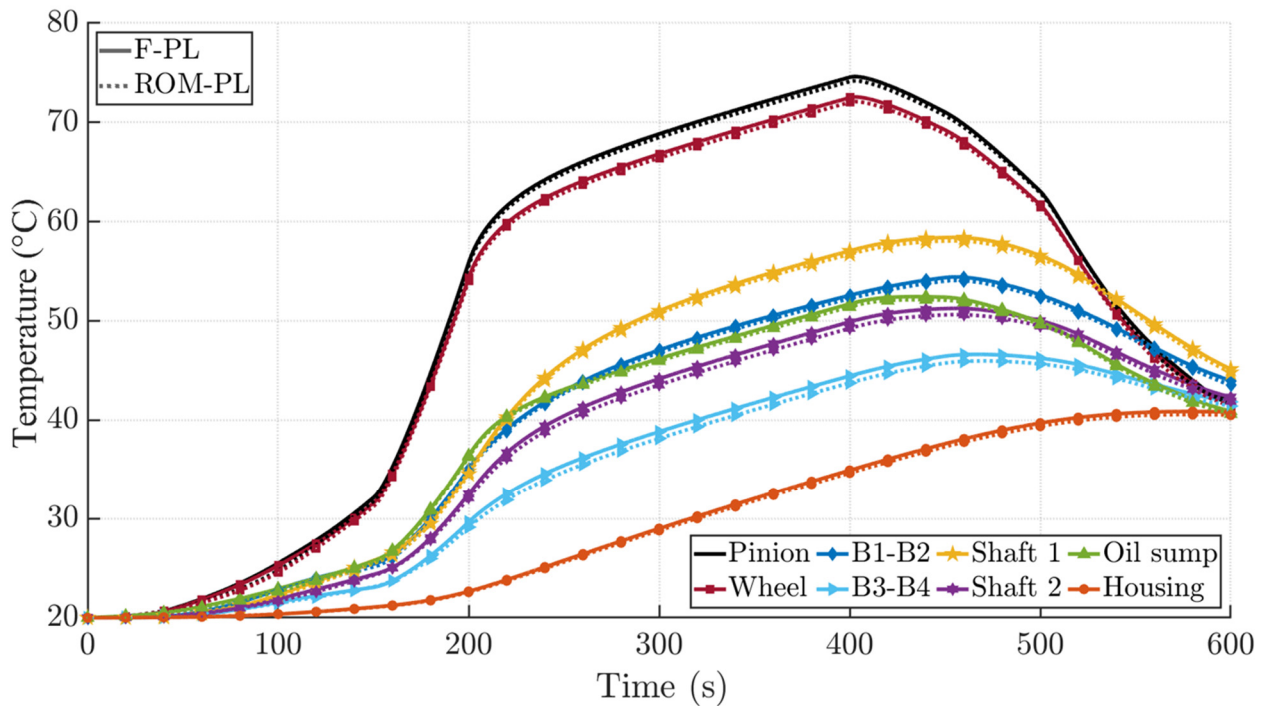


Figure 12. Component temperature during the drive cycle. Comparison between the full power loss model and the reduced order model.

The NNs provide extremely good results while drastically reducing computational time. For a 600 s drive cycle simulation, the F-PL thermal network model takes 6410 s to run (average on 5 runs), while the ROM-PL thermal network model simulation lasts only 3.8 s (average on 5 runs).

Once the numerical validation of ROM-PL within the thermal network is established, it is possible to utilise this model to test it with experimental data. The experimental data used for the study were obtained from [19], where numerous measurements of transient component temperatures were conducted. The kinematic condition is as follows: the measurements were done sequentially, beginning with the slowest circumferential speed and gradually increasing the speed after a 3 h gap. The speed levels are reported in Table 6 for clarity. This process was repeated for three different output torque levels (T_2): 0 Nm, 141 Nm, and 453 Nm.

Table 6. Kinematic condition of the experimental measurement in [19].

Kinematic Test Condition						
Time (h)	0–3	3–6	6–9	9–12	12–15	15–18
Pitch line velocity (m/s)	1	2	5	8.3	15	20
Input shaft rotational speed (rpm)	174	348	870	1444	2609	3476

Based on ISO/TR 14179-2 [21], it is anticipated that dip-lubricated gearboxes will reach a quasi-stationary temperature with respect to oil temperature after 1–3 h, depending on the design of the gearbox. The sensors were positioned at various locations, including the outer housing side surface below the oil level, inner, and outer bearing rings, shafts, gear bodies, and teeth. Furthermore, measurements were taken for the environmental temperature and the temperature of the oil sump below the oil level. Figure 13 presents both the calculated and measured temperatures of the housing, oil, bearing, and tooth bulk for the gearbox under consideration.

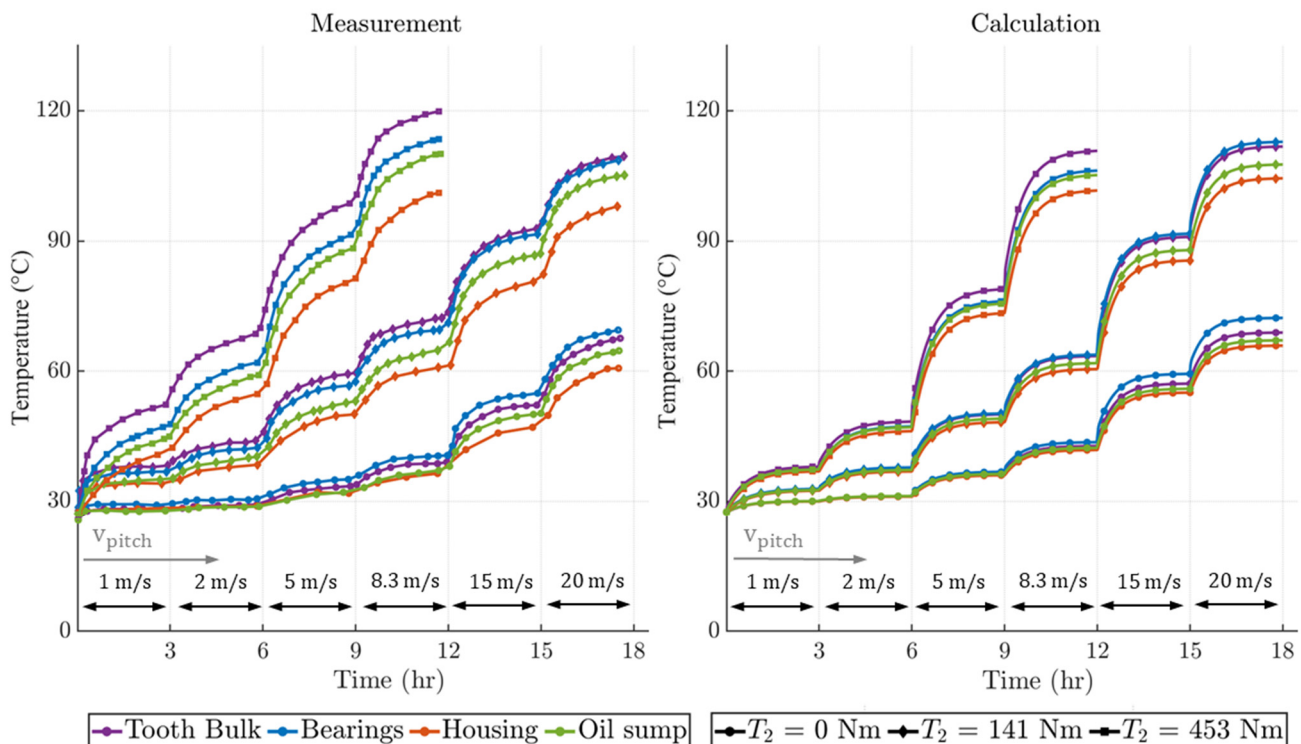


Figure 13. Comparison between temperature measurement on the FZG test rig reported in [19] (left) and the result of the ROM-PL (right).

The calculated results for the no-load and medium-load operating conditions show excellent correlation with the measured values for both temperature magnitude, gradients, and distribution among gearbox components. The discrepancy at the highest load condition is attributed to the approximated model used for the heat transfer coefficient, as

already observed in [19]. However, the degree of approximation is acceptable for a lumped parameter model. Furthermore, using the ROM-PL only 110 s of computation time were needed to simulate 18 h of operation.

7. Conclusions

An innovative methodology to estimate the thermal behaviour of the cylindrical gearbox system is presented by considering thermal sources calculated by power loss under interim operational conditions. Firstly, the power loss estimation models are tested against experimental data showing good agreement.

Once the power loss models are validated, using the Latin hypercube sampling (LHS) technique, a design of experiment (DOE) is performed to create the training and test set for the artificial neural networks (ANNs). The capability of predicting power loss of the ANNs is tested, and the authors confirm the possibility of employing these estimators to enhance simulation speed while providing accurate results. Instead of numerical simulation output, real experimental data could be used in future to train NNs.

To verify that the reduced model (ROM-PL) works correctly, using the results provided by the full model (F-PL) as a benchmark, a numerical test of a 600-s drive cycle is performed. The results of the two approaches are almost identical for the power loss and component temperatures, but the simulation time is drastically reduced. The F-PL takes 6410 s to simulate the whole drive cycle, while the ROM-PL simulation lasts only 3.8 s on average. The results provided also underline the dependence of individual losses on temperature variations. In particular, for constant torque and speed values, sliding losses tend to increase slightly with temperature due to a thinning of the lubricant film. Conversely, no-load and bearing losses decrease due to viscosity drop.

Once the numerical test of ROM-PL against F-PL leads to satisfying results, it is possible to validate this model against experimental data. The correlation between the proposed approach and the measurements in [19] is very promising and demonstrates how the implemented formulations are excellent for estimating both the components' temperature trends and the associated power losses. Furthermore, using a neural network, hours of real operation can be simulated in minutes. The noteworthy results obtained by the ROM-PL show the captivating potential of reduced-order modelling. This creates possibilities for applying this method to real-time simulations, including those associated with digital twin applications.

Author Contributions: Conceptualization, M.A., M.C., G.P. and P.P.V.; methodology, M.A., M.C., G.P. and P.P.V.; software, M.A. and G.P.; validation, M.A., M.C., G.P. and P.P.V.; formal analysis, M.A., M.C. and G.P.; investigation, M.A., M.C. and G.P.; resources, P.P.V.; data curation, M.A., M.C. and G.P.; writing—original draft preparation, M.A., M.C., G.P. and P.P.V.; writing—review and editing, M.A., M.C., G.P. and P.P.V.; visualization, M.A. and G.P.; supervision, M.C. and P.P.V.; project administration, M.C. and P.P.V.; funding acquisition, P.P.V. All authors have read and agreed to the published version of the manuscript.

Funding: This research was funded by Italian Ministry for University and Research, project “Innovative Contact Based multibody models for noise and vibration prediction in high-performance gears” grant number 202022Y4N5 and by the Italian National Center for Research on High-Performance Computing—Spoke 6 “Multiscale Modelling and Engineering Applications” MUR: CUP: E83C22003230001.

Data Availability Statement: No new data were created or analysed in this study. Data sharing is not applicable to this article.

Conflicts of Interest: The authors declare no conflict of interest. The funders had no role in the design of the study; in the collection, analyses, or interpretation of data; in the writing of the manuscript; or in the decision to publish the results.

References

1. Hohn, B.; Michaelis, K.; Vollmer, T. *Thermal Rating of Gear Drives: Balance between Power Loss and Heat Dissipation*; American Gear Manufacturers Association: Alexandria, VA, USA, 1996.
2. Aziz, A.; Höhn, B.-R.; Michaelis, K.; Hinterstoißer, M. Optimization of gearbox efficiency. *Goriva Maz. Časopis Tribol. Teh. Podmazivanja Primjen. Tekućih Plinovitih Goriva Inženjersvo Izgaranja* **2009**, *48*, 441–461.
3. Young, W.C.; Budynas, R.G. *Roark's Formulas for Stress and Strain*; McGraw-Hill: New York, NY, USA, 2002.
4. Autiero, M.; Cera, M.; Cirelli, M.; Pennestrì, E.; Valentini, P.P. Review with Analytical-Numerical Comparison of Contact Force Models for Slotted Joints in Machines. *Machines* **2022**, *10*, 966. [\[CrossRef\]](#)
5. Cirelli, M.; Valentini, P.P.; Pennestrì, E. A study of the non-linear dynamic response of spur gear using a multibody contact based model with flexible teeth. *J. Sound Vib.* **2019**, *445*, 148–167. [\[CrossRef\]](#)
6. Pennestrì, E.; Freudenstein, F. The Mechanical Efficiency of Epicyclic Gear Trains. *J. Mech. Des.* **1993**, *115*, 645–651. [\[CrossRef\]](#)
7. Esmail, E.L.; Pennestrì, E.; Cirelli, M. Power-Flow and Mechanical Efficiency Computation in Two-Degrees-of-Freedom Planetary Gear Units: New Compact Formulas. *Appl. Sci.* **2021**, *11*, 5991. [\[CrossRef\]](#)
8. Changenet, C.; Oviedo-Marlot, X.; Velez, P. Power Loss Predictions in Geared Transmissions Using Thermal Networks—Applications to a Six-Speed Manual Gearbox. *J. Mech. Des.* **2006**, *128*, 618–625. [\[CrossRef\]](#)
9. de Gevigney, J.D.; Changenet, C.; Ville, F.; Velez, P. Thermal modelling of a back-to-back gearbox test machine: Application to the FZG test rig. *Proc. Inst. Mech. Eng. Part J J. Eng. Tribol.* **2012**, *226*, 501–515. [\[CrossRef\]](#)
10. Zhou, C.; Xing, M.; Wang, H.; Hu, B. A novel thermal network model for predicting the contact temperature of spur gears. *Int. J. Therm. Sci.* **2020**, *161*, 106703. [\[CrossRef\]](#)
11. Goodfellow, I.; Yoshua, B.; Aaron, C. *Deep Learning*; MIT Press: Cambridge, MA, USA, 2016.
12. Lee, S.-H.; Park, K.-P. Development of a Prediction Model for the Gear Whine Noise of Transmission Using Machine Learning. *Int. J. Precis. Eng. Manuf.* **2023**, *1–11*. [\[CrossRef\]](#)
13. Karabacak, Y.E.; Baş, H. Experimental investigation of efficiency of worm gears and modeling of power loss through artificial neural networks. *Measurement* **2022**, *202*, 111756. [\[CrossRef\]](#)
14. Kalay, O.C.; Karpat, E.; Dirik, A.E.; Karpat, F. A One-Dimensional Convolutional Neural Network-Based Method for Diagnosis of Tooth Root Cracks in Asymmetric Spur Gear Pairs. *Machines* **2023**, *11*, 413. [\[CrossRef\]](#)
15. Wang, M.-H.; Chen, F.-H.; Lu, S.-D. Research on Fault Diagnosis of Wind Turbine Gearbox with Snowflake Graph and Deep Learning Algorithm. *Appl. Sci.* **2023**, *13*, 1416. [\[CrossRef\]](#)
16. Ezugwu, E.; Arthur, S.; Hines, E. Tool-wear prediction using artificial neural networks. *J. Mater. Process. Technol.* **1995**, *49*, 255–264. [\[CrossRef\]](#)
17. Walker, J.; Questa, H.; Raman, A.; Ahmed, M.; Mohammadpour, M.; Bewsher, S.R.; Offner, G. Application of Tribological Artificial Neural Networks in Machine Elements. *Tribol. Lett.* **2022**, *71*, 1–16. [\[CrossRef\]](#)
18. Dowson, D.; Higginson, G.R. A Numerical Solution to the Elasto-Hydrodynamic Problem. *J. Mech. Eng. Sci.* **1959**, *1*, 6–15. [\[CrossRef\]](#)
19. Paschold, C.; Sedlmair, M.; Lohner, T.; Stahl, K. Calculating component temperatures in gearboxes for transient operation conditions. *Forsch. Ingenieurwesen* **2021**, *86*, 521–534. [\[CrossRef\]](#)
20. DIN 51354. Gears—FZG Test Methods Part 1: FZG Test Method A/8.3/90 for Determining the Relative Scuffing Load Capacity of Lubricating Oils. 2006-05. Available online: https://anlagen-produktsicherheit.dmt-group.com/fileadmin/media/produktpruefung/Fluidtechnik/FZG-Test_according_to_DIN_ISO_14635.pdf (accessed on 10 June 2023).
21. ISO/TR, 141179-2; Gears—Thermal Capacity—Part 2: Thermal Load-Carrying Capacity. ISO: Geneva, Switzerland, 2001.
22. Anderson, N.E.; Loewenthal, S.H. *Spur-Gear-System Efficiency at Part and Full Load*; NASA Technical Paper No. 1622; National Aeronautics and Space Administration, Scientific and Technical Information Office: Washington, DC, USA, 1980.
23. Cirelli, M.; Valentini, P.P.; Pennestrì, E. Multibody dynamics of gear pairs: Comparison among different models. In Proceedings of the 8th ECCOMAS Thematic Conference on Multibody Dynamics, Prague, Czech Republic, 19–22 June 2017.
24. Marques, P.; Martins, R.; Seabra, J. Analytical load sharing and mesh stiffness model for spur/helical and internal/external gears—Towards constant mesh stiffness gear design. *Mech. Mach. Theory* **2017**, *113*, 126–140. [\[CrossRef\]](#)
25. Dudley, D. *Gear Handbook the Design Manufacture and Application of Gears*; McGraw-Hill: New York, NY, USA, 1962.
26. Autiero, M.; Belfiore, N.P.; Cirelli, M.; Paoli, G.; Pennestrì, E.; Valentini, P.P. A survey of empirical friction models for lubricated slotted joints in multibody dynamics simulations. In Proceedings of the ECCOMAS Thematic Conference on Multibody Dynamics, Lisbon, Portugal, 24–28 July 2023; *in press*.
27. Benedict, G.H.; Kelley, B.W. Instantaneous Coefficients of Gear Tooth Friction. *ASLE Trans.* **1961**, *4*, 59–70. [\[CrossRef\]](#)
28. Höhn, B.R.; Michaelis, K.; Otto, H.P. Flank load carrying capacity and power loss reduction by minimized lubrication. *Gear Technol.* **2011**, 53–62.
29. Arana, A.; Larrañaga, J.; Ulacia, I. Partial EHL friction coefficient model to predict power losses in cylindrical gears. *Proc. Inst. Mech. Eng. Part J J. Eng. Tribol.* **2018**, *233*, 303–316. [\[CrossRef\]](#)
30. Tallian, T. The theory of partial elastohydrodynamic. *Wear* **1972**, *21*, 49–101. [\[CrossRef\]](#)
31. Doleschel, A. Wirkungsgradberechnung von Zahnradgetrieben in Abhängigkeit vom Schmierstoff. Ph.D. Thesis, Technische Universität München, Munich, Germany, 2003.

32. Bair, S.; Winer, W.O. The high shear stress rheology of liquid lubricants at pressures of 2 to 200 MPa. *ASME J. Tribology* **1990**, *112*, 245–252. [[CrossRef](#)]
33. Concli, F.; Gorla, C. Windage, churning and pocketing power losses of gears: Different modeling approaches for different goals. *Forsch. Ingenieurwesen* **2016**, *80*, 85–99. [[CrossRef](#)]
34. Niemann, G.; Winter, H.; Höhn, B.R. *Maschinenelemente Band I*; Springer: New York, NY, USA; Berlin/Heidelberg, Germany, 1981.
35. SKF. *General Catalogue SKF*. Available online: https://www.boie.de/INTERSHOP/static/WFS/BOIE-Site/BOIE_DE/BOIE-BOIE_DE/de_DE/Kataloge/SKF/6000_I_EN.pdf (accessed on 10 June 2023).
36. SKF. Available online: <https://www.skf.com/us/products/rolling-bearings/principles-of-rolling-bearing-selection/bearing-selection-process/operating-temperature-and-speed/estimating-bearing-operating-temperature> (accessed on 10 June 2023).
37. Linke, H.; Börner, J.; Hess, R.H. *Cylindrical Gears: Calculation–Materials–Manufacturing*; Carl Hanser Verlag GmbH Co. KG: Munich, Germany, 2016.
38. Simmering, Radial-Wellendichtringe [Simmering/Radial Shaft Seals], Catalogue No. 100, Freudenberg Company: Weinheim, Germany.
39. Loh, W. On Latin hypercube sampling. *Ann. Stat.* **1996**, *24*, 2058–2080. [[CrossRef](#)]
40. Stein, M. Large Sample Properties of Simulations Using Latin Hypercube Sampling. *Technometrics* **1987**, *29*, 143. [[CrossRef](#)]
41. Choi, H.S.; An, J.; Han, S.; Kim, J.G.; Jung, J. Data-driven simulation for general-purpose multibody dynamics using Deep Neural Networks. *Multibody Syst. Dyn.* **2021**, *51*, 419–454. [[CrossRef](#)]
42. Blok, H. Theoretical Study of Temperature Rise at Surface of Actual Contact Under Oiliness Lubricating Conditions. *Proc. Inst. Mech. Eng. Gen. Discuss. Lubr. Lubr.* **1937**, *2*, 222–235.

Disclaimer/Publisher’s Note: The statements, opinions and data contained in all publications are solely those of the individual author(s) and contributor(s) and not of MDPI and/or the editor(s). MDPI and/or the editor(s) disclaim responsibility for any injury to people or property resulting from any ideas, methods, instructions or products referred to in the content.